J. Space Weather Space Clim. 2023, **13**, 31
© F. Miyake et al., Published by EDP Sciences 2023
https://doi.org/10.1051/swsc/2023030

JSWSC

Available online at:
www.swsc-journal.org

Topical Issue - Space Climate: Long-term effects of solar variability on the Earth's environment

RESEARCH ARTICLE OPEN ACCESS

No signature of extreme solar energetic particle events in high-precision ^{14}C data from the Alaskan tree for 1844–1876 CE

Fusa Miyake[1,*], Masataka Hakozaki[2], Hisashi Hayakawa[1,3,4,5], Naruki Nakano[1], and Lukas Wacker[6]

[1] Institute for Space-Earth Environmental Research, Nagoya University, Nagoya 464-8601, Japan
[2] National Museum of Japanese History, Sakura 285-8502, Japan
[3] Institute for Advanced Research, Nagoya University, Nagoya 464-8601, Japan
[4] Space Physics and Operations Division, RAL Space, Science and Technology Facilities Council, Rutherford Appleton Laboratory, Harwell Oxford, Didcot, Oxfordshire OX11 0QX, UK
[5] Nishina Centre, Riken, Wako 351-0198, Japan
[6] Laboratory for Ion Beam Physics, ETH Zürich, Zürich 8093, Switzerland

Received 31 August 2023 / Accepted 19 November 2023

Abstract – Cosmogenic nuclides – ^{14}C from tree rings and ^{10}Be and ^{36}Cl from ice cores serve as an effective proxy for past extreme solar energetic particle (SEP) events. After identifying the first signature of an extreme SEP event in 774 CE, several candidates have been found in these proxy archives, such as 993 CE, 660 BCE, and 7176 BCE. Their magnitudes have been estimated to be tens of times larger than that of the largest SEP event ever observed since the 1950s. Although a detailed survey of such extreme SEP events is ongoing, the detection of intermediate-sized SEP events that bridge the gap between modern observations and extreme events detected in cosmogenic nuclides has not progressed sufficiently, primarily because of the uncertainties in cosmogenic nuclide data. In this study, we measured ^{14}C concentrations in tree rings in the 19th century (1844–1876 CE) to search for any increases in ^{14}C concentrations corresponding to intermediate-size extreme SEP events. We utilized Alaskan tree-ring samples cut into early and latewoods to suppress the potential seasonal variations in intra-annual ^{14}C data. Notably, no significant ^{14}C variations were observed between early and latewoods (0.0 ± 0.3‰), and the annual resolution ^{14}C data series displayed an error of ~ 0.8‰. Over the entire study period, no significant increase in ^{14}C concentrations characterized by other candidates of extreme SEP events such as the 774 CE event was detected in the annual ^{14}C data. The present result imposes a constraint on the SEP fluence when the largest class of recorded solar storms occurred (especially those in 1859 CE and 1872 CE).

Keywords: Radiocarbon / Solar energetic particle / Extreme solar event / Tree ring / Carrington event

1 Introduction

Solar eruptions cause various phenomena such as geomagnetic storms and solar energetic particle (SEP) events (solar radiation storms) in the solar-terrestrial environments (Riley et al., 2018; Miyake et al., 2019; Cliver et al., 2022; Kusano, 2023). Some of these phenomena are referred to as extreme events, on the basis of their large magnitude and infrequently. In certain instances, events with once-in-a-century to once-in-a-millennium occurrences are also regarded as extreme events (Gopalswamy, 2018; Cliver et al., 2022). As these extreme events could pose enormous space-weather effects, it is essential to understand the characteristics of these extreme events, especially regarding the occurrence rate and upper magnitude limit of these events (Riley et al., 2018; Hapgood et al., 2021; Kusano, 2023). Signatures of extreme solar events that occurred beyond modern observations have been investigated using cosmogenic nuclides in the Earth's natural archives (e.g., Miyake et al., 2019; Usoskin, 2023).

Thus far, cosmogenic nuclides, namely, ^{14}C from tree rings and ^{10}Be and ^{36}Cl from ice cores, have served as proxies for past extreme SEP events (e.g., Miyake et al., 2019; Usoskin, 2023). These cosmogenic nuclides are produced by energetic particles, primarily in the stratosphere and upper troposphere (Golubenko et al., 2022), and accumulate in tree rings and ice sheets through atmospheric transportation. Despite the effects of transportation, such as the attenuation of the original signal of the energetic particles and background variation (e.g., seasonal effect on the deposition of cosmogenic nuclides), extreme SEP events that significantly exceed the background production

*Corresponding author: fmiyake@isee.nagoya-u.ac.jp

This is an Open Access article distributed under the terms of the Creative Commons Attribution License (https://creativecommons.org/licenses/by/4.0), which permits unrestricted use, distribution, and reproduction in any medium, provided the original work is properly cited.

of cosmogenic nuclides are recorded as spikes in cosmogenic nuclide datasets (Miyake et al., 2019). To date, several candidates of extreme SEP events have been discovered, e.g., those in 774 CE, 993 CE, 660 BC, and 7176 BCE as reported in previous studies (Miyake et al., 2012, 2013, 2015; Mekhaldi et al., 2015; Park et al., 2017; O'Hare et al., 2019; Brehm et al., 2022; Paleari et al., 2022).

Based on the information derived from the $^{10}Be/^{36}Cl$ ratio of ice cores, these candidates of extreme SEP events exhibit a hard energy spectrum, corresponding to events such as ground level enhancement (GLE) in February 1956 (GLE #5) and that in 2001 (GLE#69) (Mekhaldi et al., 2015; O'Hare et al., 2019; Koldobskiy et al., 2022; Paleari et al., 2022), which display the hardest energy spectra in the observed GLEs (Usoskin et al., 2020a). The SEP event in 774 CE has been estimated to be 40–100 times larger than GLE#5, which recorded the greatest flux and hardest spectra in the observational history (Cliver et al., 2022). In addition, other possible candidates of extreme SEP events have been reported in 1279 CE, 1054 CE, 5410 BCE, and 5259 BCE; whereas, these events have only been investigated through tree-ring ^{14}C records (Brehm et al., 2021; Miyake et al., 2021; Miyahara et al., 2022; Brehm et al., 2022) and await further confirmations of the origin on the basis of analyses of ice core records. Compared with the largest events (e.g., 774 CE and 7176 BCE), those at 1279 CE, 1054 CE, and 5410 BCE display small ^{14}C enhancements, i.e., ≈6‰ increase in $\Delta^{14}C$ corresponding to ≈1/3rd of the largest event (Brehm et al., 2022).

In contrast, geomagnetic storms have been measured with magnetograms since the early 19th century (e.g., Chapman & Bartels, 1940; Beggan et al., 2023). Especially from the International Geophysical Year (IGY: 1957–1958), their intensity has been quantified with the Dst index (WDC Kyoto et al., 2015). Recently, our understanding of past extreme geomagnetic storms has been considerably improved, due to the numerous studies on historical geomagnetic storms using geomagnetic measurements. So far, the greatest geomagnetic storms have been located in September 1859, February 1872, and May 1921 (Cliver et al., 2022; Hayakawa et al., 2023a,b). Further beyond, auroral records allow us to further extend our chronology back to the 10th century BCE (Hattori et al., 2019; Hayakawa et al., 2019b; Van der Sluijs & Hayakawa, 2022).

Magnitudes of extreme SEP event candidates detected so far using cosmogenic nuclides are estimated to be tens of times larger than those of the largest GLE recorded in modern observations (Mekhaldi et al., 2015; Cliver et al., 2022). As such, these events occur only once every several centuries to 24 centuries (Brehm et al., 2022), thereby rendering their classification as "extreme" extreme SEP events. According to Usoskin et al. (2023), both the occurrence distributions of SEP events, i.e., the occurrence frequencies of extreme events observed by cosmogenic nuclides data and SEP events observed in space era, can be fitted using the same Weibul distribution function. This finding signifies that the extreme events are an extension of the events detected in modern observations. However, extreme SEP events that have a magnitude in the gap between modern observations and "extreme" extreme SEP events, i.e., once in every to several centuries, have not been extensively investigated owing to several uncertainties involved in the cosmogenic nuclides data – statistical and systematic errors in measurements and insufficient separation from background fluctuations (Usoskin et al., 2020b, 2023; Usoskin & Kovaltsov, 2021). Moreover, none of the extreme events detected thus far in cosmogenic nuclides have been definitively determined to originate from extreme solar eruptions by means other than cosmogenic nuclides information (although current knowledge indicates that non-solar origins are unlikely; see Usoskin, 2023). Therefore, it is crucial to detect small enhancements of cosmogenic nuclides (corresponding to extreme SEP events) during the period that has been shown to be occurrences of extreme solar eruptions by alternative methods.

In this study, we investigated ^{14}C concentrations in tree rings from 1844 to 1876 CE to search for potential minor ^{14}C enhancements. The target period was deemed suitable for this study because of the following reasons:

1. This period accommodates the Carrington event. This event has been associated with the greatest solar flare in observational history (Cliver & Dietrich, 2013; Hudson, 2021; Hayakawa et al., 2023a);
2. This period includes at least three extreme geomagnetic storms (minimum Dst index < −500 nT; Cliver et al., 2022) on 28 August 1859 CE, 2 September 1859 CE (Carrington event; Cliver & Dietrich, 2013; Hayakawa et al., 2022a), and 4 February 1872 CE (Chapman–Silverman event; Silverman, 2008; Hayakawa et al., 2023b), as summarized in Table 1. These geomagnetic superstorms indicate relatively high solar activities and potential occurrences of extreme SEP events;
3. The background variations of the Schwabe cycle can be estimated from sunspot number (e.g., Clette et al., 2023); and
4. The ^{14}C dilution "Suess effect" caused by anthropogenic fossil fuels, is minimal (Suess 1955; Stuiver & Quay 1981).

To suppress the influence of seasonal changes of ^{14}C concentrations caused by atmospheric transportation, the ^{14}C analysis was conducted with seasonal resolution using earlywoods and latewoods.

2 Sample and methods

For this study, wood samples were obtained from *Picea sitchensis* (Bong.) Carrière (sitka spruce) from Alaska, USA (Hakozaki & Nakamura, 2013, Figs. S1 and S2). As the tree-ring width series of the sample exhibits the highest correlation with the master chronology of the Prince of Wales Island (Baillie–Pilcher t-value t_{BP} = 9.36, Baillie & Pilcher, 1973) among several Alaskan master chronologies (ITRDB, https://www.ncdc.noaa.gov/paleosearch/study/15215), we can presume that the sample was produced from the Prince of Wales Island or the surrounding region of the southeastern Alaska Pacific coastal area. We utilized two wood specimens, with sample IDs (Hakozaki & Nakamura, 2013) denoted as AKNC10 and AKNC16 for the measurement periods of 1876–1849 CE and 1851–1844 CE, respectively.

Each tree ring was segmented into earlywood and latewood using a utility knife and a graver (only the ring sample of 1849 CE from AKNC16 remained whole because of the difficulty in separating early and latewoods). Holocellulose was obtained by

Table 1. Magnitude estimations of historical solar events for geomagnetic storms (Dst estimates [nT] with the contemporaneous geomagnetic measurements), solar flares (GOES ABCMX classification defined by soft X-ray (SXR) peak intensity, e.g., X1 = 1.0×10^{-4} [W m^{-2}], Cliver et al., 2022), and SEP events (event-integrated fluence >200 MeV: F_{200} [cm^{-2}]).

Event(CE)	Geomagnetic storm (Dst estimate [nT])	Solar flare (GOES ABCMX SXR classification)	SEP (event-integrated/annual integrated F_{200} [cm^{-2}])
1872	~ −834 (Feb.) (Hayakawa et al., 2023b)	NA	$<1 \times 10^{9}$*
1859	<−600 (28 Aug.) (Hayakawa et al., 2022a) ≈ −949 ± 30 (2 Sep.) (Hayakawa et al., 2022a)	~X64.4 ± 7.2 (Cliver et al., 2022); ≈X80 (X46–X126) (Hayakawa et al., 2023a)	$<1 \times 10^{9}$*
993	NA**	NA	$4.7 \pm 1.9 \times 10^{9}$ (Usoskin et al., 2023)
774	NA	X410 ± 200 (single event, Cliver et al., 2020, 2022)	$1.1 \pm 0.3 \times 10^{10}$ (Usoskin et al., 2023)

* Upper limit from this study (2 times as large as ^{14}C errors, see the text).
** Reports for candidate aurorae are confirmed in late 992 to early 993 (Hayakawa et al., 2017a).

chemically processing the sample as follows: (1) 3 M HCl treatment at 68 °C for overnight, (2) 1.2 M NaOH treatment at 68 °C for overnight, (3) 3 M HCl at 70 °C for 3 h, (4) a bleaching treatment ($HCl/NaCl_2O$) at 77 °C for overnight and an additional bleaching treatment for a few hours until the sample color became white, (5) a neutralization with Milli-Q water, and (6) drying the sample in a drying oven. Between each procedure from (1) to (4), a Milli-Q water step for ~1 h was interposed. The wood separation and chemical treatment were performed at Nagoya University.

The holocellulose samples were graphitized using AGE at ETH Zürich (Wacker et al., 2010) and their ^{14}C concentrations were measured using the Micadas at ETH Zürich (Sookdeo et al., 2020). Each earlywood and latewood sample was measured two times to reduce uncertainties and confirm reproducibility (only the latewood 1846 CE was measured once). Brown coal (Reichwalde, Germany) was used as a process blank.

3 Results and discussion

3.1 ^{14}C data

The weighted mean of the $\Delta^{14}C$ measurements of early and latewoods across the study period from 1844–1876 CE is depicted in Figure 1a. As observed, the two measurements from the same layers were consistent with each other (Table S1). Although the layer of earlywood in 1858 CE yielded a chi-square value of 4.4 (square of differences in $\Delta^{14}C$/sum of squared errors) and was rejected at the 95 % confidence level as the layer with the weakest correspondence, it can be considered to be statistically acceptable among the total entries of ≈70 layers. Overall, the radiocarbon ages (1849–1851 CE) of AKNC10 and AKNC16 were consistent.

3.2 ^{14}C Difference between early and late woods

As depicted in Figure 1a, the distribution between earlywood and latewood resided within the margin of error. The average

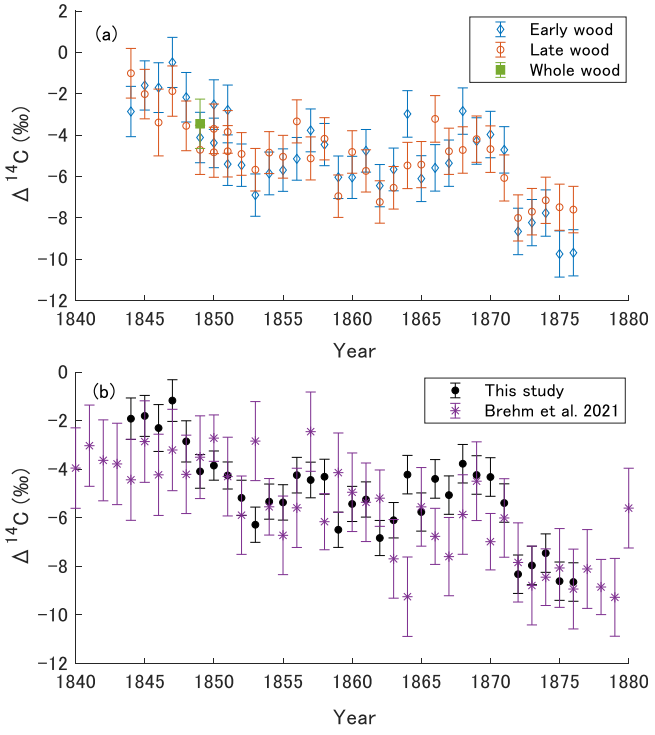

Figure 1. (a) Measured ^{14}C dataset of early and late woods (earlywood: diamonds, latewood: circles, whole wood: square). Each data point was measured twice (except for the latewood 1846 CE), and the data are expressed as the weighted average of each measurement. (b) Annual resolution ^{14}C data series (dots) compared with that reported by a previous study (stars, Brehm et al., 2021).

disparity between latewood and earlywood throughout the measurement period was 0.0 ± 0.3‰ (the error was calculated through an error propagation), and the values between the early and latewoods were not discernible even with the high precision of the measurements. Conversely, recent atmospheric ^{14}C data reveal a pronounced seasonal variation in ^{14}C concentrations, signifying that the principal stratosphere–troposphere exchange

occurs in the northern hemisphere during spring (e.g., Kitagawa et al., 2004; Levin et al., 2010; Leuenberger et al., 2018). According to the atmospheric ^{14}C data presented by Levin et al. (2010), there exists $a \approx 5‰$ $\Delta^{14}C$ increase from early spring to autumn at mid-high latitude observational points in the northern hemisphere (e.g., at Alert and Jungfraujoch stations), which corresponds to locations at similar latitudes to our Alaskan tree sample. Considering the general season of ring formation – spring to summer for earlywoods, and summer to autumn for latewoods, the present data should exhibit a difference between early and late woods in case of a similar seasonal variation in the atmosphere.

In addition to the ^{14}C data of the contemporary atmosphere, analyses of actual tree rings from the pre-industrial period have reported a difference of approximately 3‰ between earlywoods and latewoods (e.g., McDonald et al., 2019). McDonald et al. (2019) explored the possibility that the disparities between early and latewood reflect seasonal changes in the atmosphere, as well as the utilization of stored carbon in early spring (earlywood), as shown by the ^{14}C analyses of their deciduous tree samples. Since the Sitka spruce used in this study is an evergreen coniferous tree, and it is generally understood that the use of stored carbon during tree-ring formation is minimal, our results suggest the potential that early and late wood ring formation occurred within a shorter period than anticipated (for example, most of a ring may have formed intensively within 1–2 months) if a comparable ~5‰ seasonal change existed in the 19th century in the region where our tree sample grew. However, there is a report on the utilization of photosynthetic products from the previous year for Siberian Larix gmelinii (deciduous coniferous tree) based on the $^{13}CO_2$ pulse-labeling (Kagawa et al., 2006), and the utilization of longer-term stored carbon may be possible for our samples. Considering that research on seasonal changes in atmospheric ^{14}C in premodern periods, the timing of tree-ring formation, and the utilization of stored carbon across various tree species and regions is limited, additional investigations will be necessary. Specifically, to examine marginal alterations in ^{14}C (< ~5‰), understanding the characteristics of seasonal ^{14}C variations in the specific tree sample used becomes vital for eliminating uncertainties related to the seasonal variations.

3.3 ^{14}C variation from 1844–1876 CE

As we were unable to discern the difference between early and latewood in our data, we calculated the weighted average $\Delta^{14}C$ data for the same year. Figure 1b presents time series data with annual resolution, spanning from 1844 to 1876 CE, in conjunction with a recently acquired annual-resolution ^{14}C dataset (Brehm et al., 2021). Within the current dataset, the increase in ^{14}C was not significant compared to the errors (average error: 0.8‰ in $\Delta^{14}C$). Figure S3 displays a histogram of the yearly ^{14}C difference, which is fitted by a normal distribution. Here, although we did not include any additional uncertainty caused by the sample preparations (e.g., Sookdeo et al., 2020), the value of the average error is considered reasonable compared to the normal distribution parameter of yearly ^{14}C difference (1-sigma: 1.1‰, Fig. S3). Therefore, no extreme SEP event could be detected during the survey period, similar to the lower-resolution ^{14}C data from previous studies (e.g., Stuiver et al., 1998; Brehm et al., 2021) (the SEP-driven ^{14}C variation is typically characterized by a single-year elevation, followed by a sustained period of several years with high concentration data). Although a relatively steep decrease was noted after 1870 CE, this decrease may be influenced by the Suess effect. According to Stuiver and Quay (1981), the influence of fossil fuel on ^{14}C data after 1860 CE is detectable, and its impact is ≈2‰ from 1860 to 1880 CE, which aligns with the diminishing pattern observed in the present data post-1860 CE.

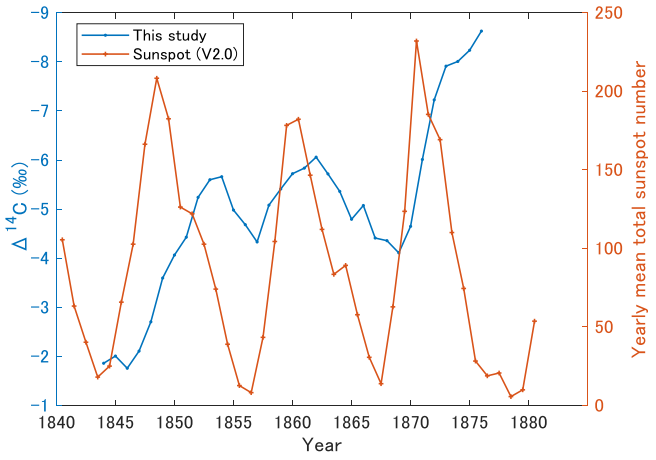

Figure 2. Comparison between sunspot records (crosses: yearly mean total sunspot number V2.0; https://www.sidc.be/SILSO/new-dataset; Clette & Lefèvre, 2016) and 3-year moving average of our ^{14}C data (dots). The period includes three solar cycles, i.e., cycle 9 (1843/07~; cycle length: 12.5 years), cycle 10 (1855/12~; cycle length: 11.2 years), and cycle 11 (1867/03 CE~; cycle length: 11.7 years), according to Table 2 of Hathaway (2015).

Figure 2 illustrates a comparison between the sunspot records and the 3-year moving average of the present dataset. The phase of an 11-year cycle is shifted by approximately 3 years in the tree-ring ^{14}C data, owing to the global carbon cycle (Siegenthaler et al., 1980; Scifo et al., 2019). Accounting for this delay in ^{14}C data, a similar cyclic fluctuation can be observed in the ^{14}C data according to sunspot variations. Consequently, the decadal variability in our ^{14}C data is deemed to reflect the Schwabe cycle (with an amplitude of 1~2 ‰), thereby indicating the absence of extreme SEP events of a magnitude that would disrupt this Schwabe cycle variation.

3.4 Relationship between extreme flare and SEP events

The three geomagnetic storm events that transpired in August and September 1859 CE and February 1872 CE, were categorized as the largest class of geomagnetic superstorms (min Dst ≤ -500 nT; Cliver et al., 2022). Specifically, the magnitudes of the geomagnetic superstorms in September 1859 and 1872 CE surpass any geomagnetic storms observed in modern times, except for the superstorm in May 1921 (Table 1 of Hayakawa et al., 2019a). The frequency of such extreme geomagnetic storm events can be estimated to be less frequent than once in every century based on the calculated Dst indices (Gopalswamy, 2018). Regarding the Carrington event in 1859 CE, a recent investigation re-estimated the flare magnitude as X80 (X46–X126) based on Carrington's original drawings for

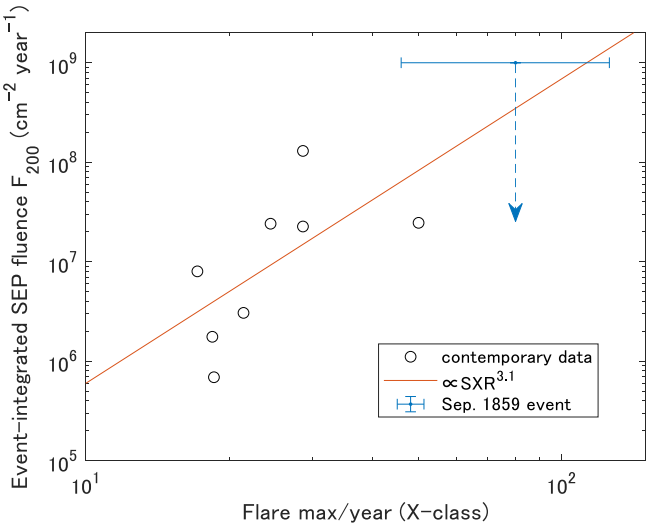

Figure 3. Relationship between SXR peak intensity of extreme solar flare (largest intensity within a year, >X10 in the previous category, https://www.sws.bom.gov.au/Educational/2/3/9) and integrated SEP fluence above 200 MeV (F_{200} [cm^{-2}], Kovaltsov et al., 2014) for the same year of the extreme solar flare, for the period from 1976 to 2020 CE (circles). The flare scale for the period 1976–2017 CE is recalibrated (i.e., the previous SXR peak intensity × 1.43) (Cliver et al., 2022). Estimations of SXR peak intensity for the Carrington events are reported in Hayakawa et al. (2023a). The arrow indicates the upper limit of F_{200} for the Carrington event (see text).

white-light flare regions and the source active regions as well as Carrington and Hodgson's reports for the flare duration and flare brightness (Hayakawa et al., 2023a). This estimation is greater than previous estimations (X64.4 ± 7.2) based on the amplitude of the resultant magnetic crochet (Cliver et al., 2022). In addition to these three geomagnetic storms occurred in August and September 1859 CE and February 1872 CE, geomagnetic data acquired by several geomagnetic observatories denote presence of extreme geomagnetic storms in October 1847 CE, October 1870, and October 1859 CE (Vaquero et al., 2008; Lakhina et al., 2012; Cliver & Dietrich 2013); which requires further future investigations.

Consequently, we deduced that intense solar activity caused extremely large-scale solar flares and geomagnetic storms during the survey period of this study, and a significant volume of SEP accordingly reached the Earth. Owens et al. (2022) highlighted that the "event-by-event correspondence" between geomagnetic storms and GLEs is low when utilizing datasets of the modern era. However, higher solar activities are inclined to generate large-scale solar flares, and therefore, extensive magnetic storms and GLEs.

The magnitudes of extreme solar flares of ≥X14.3 (≥X10: unrecalibrated classification in GOES data prior to GOES16, https://www.sws.bom.gov.au/Educational/2/3/9; see also Cliver et al., 2022; Machol et al., 2022) occurring after 1976 CE (considered the largest flare if several extreme flares occurred in the same year) and cumulative F_{200} [MeV] values from GLEs (Kovaltsov et al., 2014) occurring in the same year as the extreme solar flares are comparatively presented in Figure 3. Herein, we assumed that a large-scale event occurred in the same year, even in the case of a weak one-to-one relationship between flares and SEP events. In addition to the modern data, the upper limit of the cumulative F_{200} in 1859 CE derived herein is exhibited in Figure 3. Here, the upper limit is assumed to be two times the ^{14}C average error and scaled to the total ^{14}C increment of the 774 CE event, i.e., 17.6‰ (Brehm et al., 2022), using an estimated F_{200} value for the 774 CE event (Usoskin et al., 2023; Table 1). We observed that the upper limit does not deviate from a fitted power function of the modern data. Although the present samples did not display any significant increase in ^{14}C concentrations after 1859 CE, a significant yet marginal ^{14}C enhancement has been confirmed in a tree sample collected from a substantially high latitude in Finland, which may be correlated to SEPs (Uusitalo et al., private communications). To confirm this possibility, further investigation may yield the SEP fluence of the Carrington event, whereas we need ice core datasets (^{10}Be and ^{36}Cl) and higher precision tree-ring ^{14}C datasets.

4 Conclusions

This study conducted high-precision ^{14}C measurements to investigate the increases in ^{14}C concentrations caused by intermediate SEP events between GLEs and "extreme" extreme SEP events detected by modern observations and cosmogenic nuclides, respectively. The analysis utilized Sitka spruce tree-ring samples from Alaska for the period spanning from 1844 to 1876 CE, during which several extreme geomagnetic storms and the Carrington solar flare (1859 and 1872 CE) occurred. As conventional ^{14}C analyses in annual tree rings (viz. time resolution of one year) can be affected by variations in the scale of a few permil of ^{14}C induced by the seasonal atmospheric alteration in ^{14}C concentrations owing to stratosphere–troposphere transportation, we carefully segmented the early and latewoods to minimize this influence. In the ^{14}C data of the Sitka spruce sample between early and latewoods, no significant difference was observed with high accuracy ($\Delta^{14}C$ difference: 0.0 ± 0.3‰), alluding to the possibility that tree-ring formation transpired in a briefer period than anticipated. Further investigations concerning the seasonal change in various species across expansive regions are required to deem the seasonal variations in ^{14}C concentrations as a background fluctuation of marginal variations in ^{14}C concentrations.

In the obtained annual ^{14}C series, no significant increase in ^{14}C concentrations was detected with respect to the errors (average error: 0.8‰). The error of the ^{14}C data obtained herein was approximately 1/20th of the total increase in ^{14}C concentrations for the 774 CE event (17.6‰; Brehm et al., 2022), which represents the largest class in the Holocene. We distinguished fine structures in the ^{14}C data, which were consistent with the Schwabe cycle estimated from the sunspot data, implying that no SEP event occurred during the survey period that would disrupt the ^{14}C fluctuations caused by the Schwabe cycle with an amplitude of ~1–2‰. Concerning the Carrington event in September 1859 CE, which is associated with one of the largest flares and geomagnetic storms on record, the upper limit (detection limit) of the SEP event obtained herein is in accord with the magnitude of the SEP event projected from contemporary data. Thus, it is not unexpected that SEP events exist slightly beneath the detection threshold. Although we did not detect any indicators of an extreme SEP event in the three

pronounced solar events in the 19th century, previous research has documented more signatures of extreme solar storms in other periods (e.g., 1770, 1903, and 1909 CE: Hayakawa et al., 2017b, 2019c, 2020). Therefore, we might uncover intermediate-size extreme SEP events that are detectable with the current measurement precision in these ages.

Supplementary material

The supplementary material of this article is available at https://www.swsc-journal.org/10.1051/swsc/2023030/olm.

Acknowledgements. We thank Shozo Ohta for the sample preparation. We thank the ISSI international team activity (#510; SEESUP). F.M.'s fork was supported by JSPS Grant-in-Aids JP20K20918, JP20H05643, JP20H00035, JP20H01369, and JP19H00706. H.H. thanks JSPS Grant-in-Aids JP20K22367, JP20H05643, JP21K13957, and JP22K02956, JSPS Overseas Challenge Program for Young Researchers, the ISEE director's leadership fund for FYs 2021–2023, Young Leader Cultivation (YLC) program of Nagoya University, Tokai Pathways to Global Excellence (Nagoya University) of the Strategic Professional Development Program for Young Researchers (MEXT), and the young researcher units for the advancement of new and undeveloped fields by Institute for Advanced Research of Nagoya University (the Program for Promoting the Enhancement of Research Universities). H.H. thanks the WDC SILSO for providing the sunspot number and the Oulu University for providing the International GLE database. The editor thanks Timothy Jull and an anonymous reviewer for their assistance in evaluating this paper.

References

Baillie MGL, Pilcher JR. 1973. A simple crossdating program for tree-ring research. *Tree-Ring Bull.* **33**: 7–14.

Beggan CD, Eaton E, Maume E, Clarke E, Williamson J, et al. 2023. Digitizing UK analogue magnetogram records from large geomagnetic storms of the past two centuries. *Geosci Data J* **10**: 73–86. https://doi.org/10.1002/gdj3.151.

Brehm N, Bayliss A, Christl M, Synal H-A, Adolphi F, et al. 2021. Eleven-year solar cycles over the last millennium revealed by radiocarbon in tree rings. *Nat Geosci* **14**: 10–15. https://doi.org/10.1038/s41561-020-00674-0.

Brehm N, Christl M, Knowles TDJ, Casanova E, Evershed RP, et al. 2022. Tree-rings reveal two strong solar proton events in 7176 and 5259 BCE. *Nat Commun* **13**: 1196. https://doi.org/10.1038/s41467-022-28804-9.

Chapman S, Bartels J. 1940. *Geomagnetism, Vol. I: Geomagnetic and Related Phenomena*. Oxford University Press, London. https://ui.adsabs.harvard.edu/abs/1940gm1.book..C/abstract.

Clette F, Lefèvre L. 2016. The new sunspot number: assembling all corrections. *Sol Phys* **291**: 2629–2651. https://doi.org/10.1007/s11207-016-1014-y.

Clette F, Lefèvre L, Chatzistergos T, Hayakawa H, Carrasco VMS, et al. 2023. Recalibration of the sunspot-number: status report. *Sol Phys* **298**: 44. https://doi.org/10.1007/s11207-023-02136-3.

Cliver EW, Dietrich WF. 2013. The 1859 space weather event revisited: limits of extreme activity. *J Space Weather Space Clim* **3**: A31. https://doi.org/10.1051/swsc/2013053.

Cliver EW, Hayakawa H, Love JJ, Neidig DF. 2020. On the size of the flare associated with the solar proton event in 774 AD. *ApJ* **903**: 41. https://doi.org/10.3847/1538-4357/abad93.

Cliver EW, Schrijver CJ, Shibata K, Usoskin IG. 2022. Extreme solar events. *Living Rev Sol Phys* **19**: 2. https://doi.org/10.1007/s41116-022-00033-8.

Golubenko K, Rozanov E, Kovaltsov G, Usoskin I. 2022. Zonal mean distribution of cosmogenic isotope (^{7}Be, ^{10}Be, ^{14}C, and ^{36}Cl) production in stratosphere and troposphere. *J Geophys Res Atmos* **127**: e2022JD036726. https://doi.org/10.1029/2022JD036726.

Gopalswamy N. 2018. Chapter 2 – Extreme solar eruptions and their space weather consequences. In: *Extreme Events in Geospace: Origins, Predictability, and Consequences*. Buzulukova N, (Ed.) Elsevier, Amsterdam. https://doi.org/10.1016/B978-0-12-812700-1.00002-9.

Hakozaki M, Nakamura T. 2013. *Tree-ring dating and dendroprovenancing of the imported Spruce woods*. Bull. Nagoya Univ. Museum No. 29, 1–11, in Japanese. https://doi.org/10.18999/bulnum.029.01.

Hapgood M, Angling MJ, Attrill G, Bisi M, Cannon PS, et al. 2021. Development of space weather reasonable worst case scenarios for the UK National Risk Assessment. *Space Weather* **19**: e2020SW002593. https://doi.org/10.1029/2020SW002593.

Hathaway DH. 2015. The solar cycle. *Living Rev Sol Phys* **12**: 4. https://doi.org/10.1007/lrsp-2015-4.

Hattori K, Hayakawa H, Ebihara Y. 2019. Occurrence of great magnetic storms on 6–8 March 1582. *Mon Not R Astron Soc* **487(3)**: 3550–3559. https://doi.org/10.1093/mnras/stz1401.

Hayakawa H, Tamazawa H, Uchiyama Y, Ebihara Y, Miyahara H. 2017a. Historical aurora evidences for great magnetic storms in 990s. *Sol Phys* **292**: 12. https://doi.org/10.1007/s11207-016-1039-2.

Hayakawa H, Iwahashi K, Ebihara Y, Tamazawa H, Shibata K, et al. 2017b. Long-lasting extreme magnetic storm activities in 1770 found in historical documents. *Astrophys J Lett* **850**: L31. https://doi.org/10.3847/2041-8213/aa9661.

Hayakawa H, Ebihara Y, Willis DM, Toriumi S, Iju T, et al. 2019a. Temporal and spatial evolutions of a large sunspot group and great auroral storms around the Carrington Event in 1859. *Space Weather* **17**: 1553–1569. https://doi.org/10.1029/2019SW002269.

Hayakawa H, Mitsuma Y, Ebihara Y, Miyake F. 2019b. The earliest candidates of auroral observations in Assyrian Astrological Reports: Insights on solar activity around 660 BCE. *Astrophys J Lett* **884**: L18. https://doi.org/10.3847/2041-8213/ab42e4.

Hayakawa H, Ebihara Y, Cliver EW, Hattori K, Toriumi S, et al. 2019c. The extreme space weather event in September 1909. *Mon Not R Astron Soc* **484**: 4083–4099. https://doi.org/10.1093/mnras/sty3196.

Hayakawa H, Ribeiro P, Vaquero JM, Gallego MC, Knipp DJ, et al. 2020. The extreme space weather event in 1903 October/November: An outburst from the quiet Sun. *Astrophys J Lett* **897**: L10. https://doi.org/10.3847/2041-8213/ab6a18.

Hayakawa H, Nevanlinna H, Blake SP, Ebihara Y, Bhaskar AT, et al. 2022a. Temporal variations of the three geomagnetic field components at Colaba Observatory around the Carrington Storm in 1859. *Astrophys J* **928**: 32. https://doi.org/10.3847/1538-4357/ac2601.

Hayakawa H, Bechet S, Clette F, Hudson H, Maehara H, et al. 2023a. Magnitude estimates for the Carrington Flare in 1859 September: as seen from the original records. *Astrophys J Lett* **954**: L3. https://doi.org/10.3847/2041-8213/acd853.

Hayakawa H, Cliver EW, Clette F, Ebihara Y, Toriumi S, et al. 2023b. The extreme space weather event of February 1872: Sunspots, magnetic disturbance, and auroral displays. *ApJ* **959**: 23. https://doi.org/10.3847/1538-4357/acc6cc.

Hudson HS. 2021. Carrington events. *Annu Rev Astron Astrophys* **59**: 445–477. https://doi.org/10.1146/annurev-astro-112420-023324.

Kagawa A, Sugimoto A, Maximov TC. 2006. 13CO2 pulse-labelling of photoassimilates reveals carbon allocation within and between tree rings. *Plant Cell Environ* **29(8)**: 1571–1584. PMID: 16898018. https://doi.org/10.1111/j.1365-3040.2006.01533.x.

Kitagawa H, Mukai H, Nojiri Y, Shibata Y, Kobayashi T, et al.et al. 2004. Seasonal and secular variations of atmospheric $^{14}CO_2$ over the Western Pacific since 1994. *Radiocarbon* **46(2)**: 901–910.

Koldobskiy S, Usoskin I, Kovaltsov GA. 2022. Effective energy of cosmogenic isotope (^{10}Be, ^{14}C and ^{36}Cl) production by solar energetic particles and galactic cosmic rays. *J Geophys Res Space Phys* **127**: e2021JA029919. https://doi.org/10.1029/2021JA029919.

Kovaltsov GA, Usoskin IG, Cliver EW, Dietrich WF, Tylka AJ. 2014. Fluence ordering of solar energetic proton events using cosmogenic radionuclide data. *Sol Phys* **289**: 4691–4700. https://doi.org/10.1007/s11207-014-0606-7.

Kusano K. 2023. *Solar-terrestrial environmental prediction*. Springer Nature Singapore, Singapore.

Lakhina GS, Alex S, Tsurutani BT, Gonzalez WD. 2012. Supermagnetic storms: Hazard to Society. In: *Extreme events and natural hazards: the complexity perspective*. Sharma AS, Bunde A, Dimri VP, Baker DN (Eds.), American Geophysical Union, Washington, DC. https://doi.org/10.1029/2011GM001073.

Leuenberger M, Levin I, Hammer S. 2018. Long-term observations of $^{14}CO_2$ at Jungfraujoch. Activity Report 2018. International Foundation HFSJG.

Levin I, Naegler T, Kromer B, Diehl M, Francey RJ, et al. 2010. Observations and modelling of the global distribution and long-term trend of atmospheric $^{14}CO_2$. *Tellus B Chem Phys Meteorol* **62(1)**: 26–46. https://doi.org/10.1111/j.1600-0889.2009.00446.x.

Machol J, Viereck R, Peck C, Mothersbaugh J III. 2022. *GOES X-ray Sensor (XRS) Operational Data (Version 1.5)*. Stennis Space Center, NOAA.

McDonald L, Chivall D, Miles D, Bronk Ramsey C. 2019. Seasonal variations in the ^{14}C content of tree rings: influences on radiocarbon calibration and single-year curve construction. *Radiocarbon* **61(1)**: 185–194. https://doi.org/10.1017/RDC.2018.64.

Mekhaldi F, Muscheler R, Adolphi F, Aldahan A, Beer J, et al. 2015. Multiradionuclide evidence for the solar origin of the cosmic-ray events of AD 774/5 and 993/4. *Nat Commun* **6(1)**: 8611. https://doi.org/10.1038/ncomms9611.

Miyake F, Nagaya K, Masuda K, Nakamura T. 2012. A signature of cosmic-ray increase in AD 774–775 from tree rings in Japan. *Nature* **486(7402)**: 240–242. https://doi.org/10.1038/nature11123.

Miyake F, Masuda K, Nakamura T. 2013. Another rapid event in the carbon-14 content of tree rings. *Nat Commun* **4(1)**: 1748. https://doi.org/10.1038/ncomms287310.1038/ncomms2783.

Miyake F, Suzuki A, Masuda K, Horiuchi K, Motoyama H, et al. 2015. Cosmic ray event of A.D. 774–775 shown in quasi-annual 10Be Data from the Antarctic Dome Fuji Ice Core. *Geophys Res Lett* **42**: 84–89. https://doi.org/10.1002/2014GL062218.

Miyake F, Usoskin IG, Poluianov S (Eds.). 2019. *Extreme Solar Particle Storms*. IOP Publishing, Bristol, United Kingdom. https://doi.org/10.1088/2514-3433/ab404a.

Miyake F, Panyushkina IP, Jull AJT, Adolphi F, Brehm N, et al. 2021. A single-year cosmic ray event at 5410 BCE registered in 14C of tree rings. *Geophys Res Lett* **48**: e2021GL093419. https:/doi.org/10.1029/2021GL093419.

Miyahara H, Tokanai F, Moriya T, Takeyama M, Sakurai H, et al. 2022. Recurrent large-scale solar proton events before the onset of the Wolf Grand solar minimum. *Geophys. Res. Lett.* **49**: e2021GL097201. https://doi.org/10.1029/2021gl097201.

O'Hare P, Mekhaldi F, Adopphi F, Raisbeck G, Aldahan A, et al. 2019. Multiradionuclide evidence for an extreme solar proton event around 2,610 B.P. (~660 BC). *Proc Natl Acad. Sci* **116**: 5961–5966. https://doi.org/10.1073/pnas.181572511.

Owens MJ, Barnard LA, Pope BJS, Lockwood M, Usoskin I, et al. 2022. Solar energetic-particle ground-level enhancements and the solar cycle. *Sol Phys* **297**: 105. https://doi.org/10.1007/s11207-022-02037-x.

Paleari CI, Mekhaldi F, Adolphi F, Christl M, Vockenhuber C, et al. 2022. Cosmogenic radionuclides reveal an extreme solar particle storm near a solar minimum 9125 years BP. *Nat Commun* **13**: 214. https://doi.org/10.1038/s41467-021-27891-4.

Park J, Southon J, Fahrni S, Creasman PP, Mewaldt R. 2017. Relationship between solar activity and Δ^{14}C peaks in AD 775, AD 994, and 660 BC. *Radiocarbon* **59**: 1147–1156. https://doi.org/10.1017/RDC.2017.59.

Riley P, Baker D, Liu YD, Verronen P, Singer H, Güdel M. 2018. Extreme space weather events: from cradle to grave. *Space Sci Rev* **214**: 21. https://doi.org/10.1007/s11214-017-0456-3.

Scifo A, Kuitems M, Neocleous A, Pope BJS, Miles D, et al. 2019. Radiocarbon production events and their potential relationship with the Schwabe Cycle. *Sci Rep* **9**: 17056. https://doi.org/10.1038/s41598-019-53296-x.

Siegenthaler U, Heimann M, Oeschger H. 1980. 14C variations caused by changes in the global carbon cycle. *Radiocarbon* **22(2)**: 177–191. https://doi.org/10.1017/S0033822200009449.

Silverman SM. 2008. Low-latitude auroras: The great aurora of 4 February 1872. *J Atmos Sol-Terr Phys* **70**: 1301–1308. https://doi.org/10.1016/j.jastp.2008.03.012.

Sookdeo A, Kromer B, Büntgen U, Friedrich M, Friedrich R, et al. 2020. Quality dating: a well-defined protocol implemented at ETH for high-precision ^{14}C-dates tested on late glacial wood. *Radiocarbon* **62(4)**: 891–899. https://doi.org/10.1017/RDC.2019.132.

Stuiver M, Quay PD. 1981. Atmospheric ^{14}C changes resulting from fossil fuel CO_2 release and cosmic ray flux variability. *Earth Planet Sci Lett* **53**: 349–362.

Stuiver M, Reimer PJ, Braziunas TF. 1998. High-precision radiocarbon age calibration for terrestrial and marine samples. *Radiocarbon* **40(3)**: 1127–1151. https://doi.org/10.1017/S0033822200019172.

Suess HE. 1955. Radiocarbon concentration in modern wood. *Science* **122**: 415.

Usoskin IG. 2023. A history of solar activity over millennia. *Living Rev Sol Phys* **20**: 2. https://doi.org/10.1007/s41116-023-00036-z.

Usoskin IG, Kovaltsov GA. 2021. Mind the gap: New precise ^{14}C data indicate the nature of extreme solar particle events. *Geophys Res Lett* **48**: e94848. https://doi.org/10.1029/2021GL094848.

Usoskin I, Koldobskiy S, Kovaltsov GA, Gil A, Usoskina I, et al. 2020a. Revised GLE database: Fluences of solar energetic particles as measured by the neutron-monitor network since 1956. *A&A* **640**: A17. https://doi.org/10.1051/0004-6361/202038272.

Usoskin IG, Koldobskiy SA, Kovaltsov GA, Rozanov EV, Sukhodolov TV, et al. 2020b. Revisited reference solar proton event of 23 February 1956: Assessment of the cosmogenic-isotope method sensitivity to extreme solar events. *J Geophys Res Space Phys* **125**: e27921. https://doi.org/10.1029/2020JA027921.

Usoskin IG, Koldobskiy SA, Poluianov SV, Raukunen O, Vainio R, et al. 2023. Consistency of the average flux of solar energetic particles over timescales of years to megayears. *A&A* **670**: L22. https://doi.org/10.1051/0004-6361/202245810.

Van der Sluijs MA, Hayakawa H. 2022. A candidate auroral report in the Bamboo Annals, indicating a possible extreme space weather event in the early 10th century BCE. *Adv Space Res*. https://doi.org/10.1016/j.asr.2022.01.010.

Vaquero JM, Valente MA, Trigo RM, Ribeiro P, Gallego MC. 2008. The 1870 space weather event: Geomagnetic and auroral records. *J Geophys Res Space Phys* **113**: A08230. https://doi.org/10.1029/2007JA012943.

Wacker L, Nemec M, Bourquin J. 2010. A revolutionary graphitisation system: fully automated, compact and simple. *Nucl Instrum Methods Phys Res Sect B* **268**: 931–934.

WDC Kyoto, Nose M, Iyemori T, Sugiura M, Kamei T. 2015. *Geomagnetic Dst Index*. https://doi.org/10.17593/14515-74000.

Cite this article as: Miyake F, Hakozaki M, Hayakawa H, Nakano N & Wacker L, 2023. No signature of extreme solar energetic particle events in high-precision ^{14}C data from the Alaskan tree for 1844–1876 CE. *J. Space Weather Space Clim*. **13**, 31. https://doi.org/10.1051/swsc/2023030.